
Once-for-All: Controllable Generative Image Compression with Dynamic Granularity Adaption

Anqi Li^{1,2} Yuxi Liu^{1,2} Huihui Bai^{1,2,*} Feng Li^{3,*} Runmin Cong⁴ Meng Wang³ Yao Zhao^{1,2}

¹ Institute of Information Science, Beijing Jiaotong University

² Beijing Key Laboratory of Advanced Information Science and Network Technology

³ School of Computer Science and Engineering, Hefei University of Technology

⁴ School of Control Science and Engineering, Shandong University

{lianqi, yuxiliu, hhbai, yzhao}@bjtu.edu.cn

fengli@hfut.edu.cn rmcong@sdu.edu.cn eric.mengwang@gmail.com

Abstract

Although recent generative image compression methods have demonstrated impressive potential in optimizing the rate-distortion-perception trade-off, they still face the critical challenge of flexible rate adaption to diverse compression necessities and scenarios. To overcome this challenge, this paper proposes a **Controllable Generative Image Compression** framework, **Control-GIC**, the first capable of fine-grained bitrate adaption across a broad spectrum while ensuring high-fidelity and generality compression. We base **Control-GIC** on a VQGAN framework representing an image as a sequence of variable-length codes (*i.e.* VQ-indices), which can be losslessly compressed and exhibits a direct positive correlation with the bitrates. Therefore, drawing inspiration from the classical coding principle, we naturally correlate the information density of local image patches with their granular representations, to achieve dynamic adjustment of the code quantity following different granularity decisions. This implies we can flexibly determine a proper allocation of granularity for the patches to acquire desirable compression rates. We further develop a probabilistic conditional decoder that can trace back to historic encoded multi-granularity representations according to transmitted codes, and then reconstruct hierarchical granular features in the formalization of conditional probability, enabling more informative aggregation to improve reconstruction realism. Our experiments show that **Control-GIC** allows highly flexible and controllable bitrate adaption and even once compression on an entire dataset to fulfill constrained bitrate conditions. Experimental results demonstrate its superior performance over recent state-of-the-art methods.

1 Introduction

Lossy image compression complies with the rate-distortion criterion in Shannon’s theorem [43], which aims to pursue minimal storage of images without quality sacrifice. Traditional standardized codecs [48, 44, 7] adhere to a typical hand-crafted “transforming-quantization-entropy coding” rule, showing substantial performance on generic images. Learnable compression algorithms [4, 5, 37, 38] follow a similar pipeline that parameterizes it as convolutional neural networks (CNNs) operating on latent variables with end-to-end R-D optimization. Recent works [42, 47, 2, 36] leverage the generation capability of generative adversarial networks (GANs) [18] to deal with the compression

* Corresponding Authors

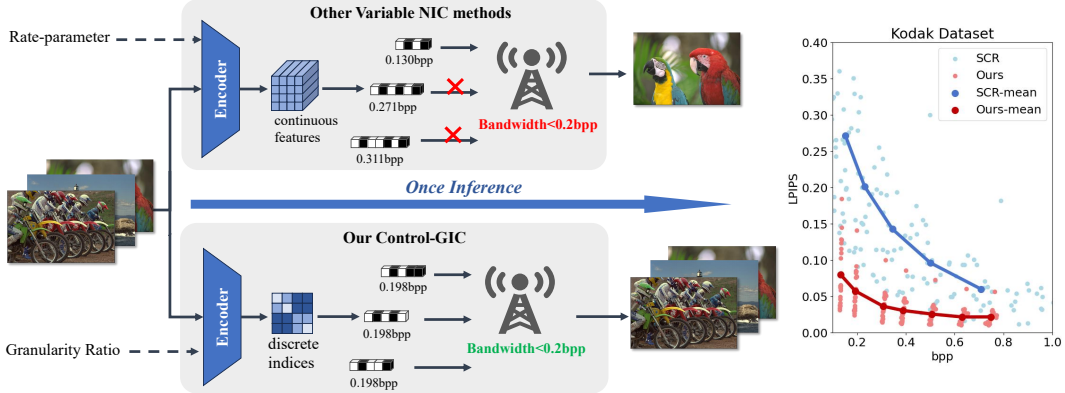


Figure 1: Our Control-GIC achieves controllable target bit rates in a single inference, making it easier and more practical to adapt to different bandwidth requirements than other variable bit rate methods. The right figure shows that our average LPIPS is much lower (see Ours-mean), and each image is well-controlled near the target rate than the MSE-based variable method SCR [32].

task, known as generative image compression, which minimizes the distribution divergence between original and reconstructed images, resulting in perfect perceptual quality. However, these methods train the models separately for specific R-D points with Lagrange multiplier (λ)-weighted R-D loss, each corresponding to an individual λ . In this way, multiple fixed-rate models are necessitated to vary bitrates, resulting in dramatic computational costs and inefficient deployment to cater to diverse bitrates and devices. Some CNN-based models propose to learn scalable bitstreams [27, 46, 3, 35, 52, 25] or truncated quantization parameters to control the bitrates [45, 14, 50, 15]. On the one hand, these models typically support a restricted range of bitrates with substantial variance distribution, thereby constraining their adaptability to finer bitrate adjustments. On the other hand, they tend to quantify the distortion using the pixel-wise mean square error (MSE), which is inconsistent with human perception and often yields implausible reconstruction, particularly at low bitrates [8, 36]. There are several methods that introduce the scalable [24] or variable-rate [19] designs into generative models. While they have achieved remarkable improvements in perceptual quality, the models are still constrained by finite compression rates.

In the light of the preceding discussion, in this work, we propose an innovative generative image compression paradigm, dubbed Control-GIC, which accommodates highly flexible and fine-grained controls on a broad range of bitrates and perceptually realistic reconstruction with solely one set of optimized weights. Motivated by that VQ-based models [17, 55] enable to encode images into discrete codes that represent the local visual patterns, Control-GIC hybridizes the classical coding principle in the architecture with VQGAN to relax the typical R-D optimization and provide a controllable unified generative model. Specifically, Control-GIC first characterizes the inherent information density and context complexity of local image patches as the information entropy. We devise the granularity-informed encoder that determines the granularity of these patches based on their entropy values, which are represented by sequential variable-length codes (*i.e.*, VQ-indices) based on the learned codebook prior (see Figure 1). One can flexibly control the statistics of the granularities to adjust the VQ-indices of patches dynamically adapting to diverse desirable bitrates. As correlated to the regional information of images, the VQ-indices are spatially variant to adapt to the local contents. We then develop a statistical entropy coding module, which is no-parametric and captures the code distribution in the learned codebook prior across a large-scale natural dataset to approximate a generalized probability distribution, encoding the VQ-indices losslessly and more compactly during inference, improving the compression efficiency. On top of entropy coding, a probabilistic conditional decoder is further developed, which formalizes the reconstruction of granular features in a conditional probability manner leveraging the historic encoded multi-granularity representations given entropy-decoded indices. Our comprehensive experimental results demonstrate the outstanding adaption capability of the proposed Control-GIC by achieving superior performance from perceptual quality, distortion quality, and non-reference quality perspectives compared with three types of recent state-of-the-art methods including generative, progressive, and variable-rate compression methods using only a single unified model.

The main contributions of this work are three-fold:

- We propose the Control-GIC, a unified generative compression model capable of variable bitrate adaption across a broad spectrum while preserving high-perceptual fidelity reconstruction. To our best knowledge, this is the first that allows highly flexible and controllable bitrate adaption and even once compression on an entire dataset to fulfill constrained bitrate conditions.
- We propose a granularity-inform encoder that represents the image patches of sequential spatially variant VQ-indices to support fine-grained variable rate controlling and adaption. Besides, a non-parametric statistical entropy coding is introduced to encode the VQ-indices losslessly based on the approximation of the code distribution in the learned codebook prior across a large-scale natural dataset.
- We design a probabilistic conditional decoder, which aggregates historic encoded multi-granularity representations to reconstruct hierarchical granular features in a conditional probability manner, achieving realism improvements.

2 Related work

Neural Image Compression Transformation, quantization, and entropy coding are three key components in neural image compression (NIC). Since Ballé *et al.* [4] propose the pioneering learnable NIC method using convolutional neural network (CNN), later methods make improvements in transformation to learn a more compact and exact representation with efficient architecture designs [13, 49, 56]. With the help of hyperprior and context models [5, 31, 40], the entropy model captures more precise spatial dependencies in the latent, helping probability distribution estimation.

Inspired by the GANs [18] and Diffusion Model (DM) [22] in various image processing tasks, some algorithms [47, 2, 41, 42, 36, 23, 51] incorporate generative models into NIC frameworks. For instance, Agustsson *et al.* [2] uses GAN loss along with R-D loss to achieve end-to-end full-resolution image compression while giving dramatic bitrate savings. Mentzer *et al.* [36] incorporates GAN with compression architecture systematically and generates robust perceptual evaluation. Hoogetboom *et al.* [23] explore autoregressive diffusion model to achieve competitive lossless compression evaluated on a small image dataset. Yang *et al.* [51] propose an end-to-end DM-based compression framework and reconstruct images through the reverse diffusion process conditioned with context information, achieving competitive performance compared to some GAN-based compression methods. Superisely, VQGAN [17]-based generative techniques have shown impressive performance for learning strong codebook priors to discretely represent the visual features in image synthesis, which provides new inspiration to image compression. Mao *et al.* [34] introduce VQ-indices compression based on the VQGAN model to achieve simple but efficient compression, significantly improving the compression ratio. Based on these observations, we further unleash the potential of VQ and build custom designs around VQGAN to achieve controllable generative compression accommodating general bitrates via a unified single model.

Rate-Adaption NIC The aforementioned methods often face the challenge of deployment in resource-limited devices they are trained as separate models for specific bitrates, which increases the complexity overhead to support multiple bitrates. Current research solving such a rate adaption problem can be roughly divided into two categories: variable-rate compression [12, 33, 15, 20] and progressive compression [46, 35, 30, 25, 52]. For the former, Theis *et al.* [46] propose to learn rate-specific scalar parameters to scale the transformed features before quantization. Choi *et al.* [14] present a conditional convolution that adaptively learns the scale and shift factors from a one-shot vector to compress the image for different target quality levels. Cai *et al.* [10] stack multi-scale representations to perform content-adaptive rate allocation. Yang *et al.* [50] leverage slimmable neural networks to perform low- and high-rate compression using partial and all parameters respectively. In [15], Cui *et al.* incorporate gain units that guide the network to allocate bits on specific channels as well as control rates. Lee *et al.* [32] present a selective compression approach that performs entropy coding only for the partially selected latent representations via 3D binary masks.

Progressive compression aims to learn a scalable bitstream that can be progressively exploited to compress images from low to high bitrates. Torderici *et al.* [46] develop a full-resolution recurrent network to transmit bits progressively for high-resolution image compression. Johnston *et al.* [27]

introduce an effective initialization scheme for the hidden states of RNN and provide a spatially adaptive rate controller. Zhang *et al.* [52] propose to explore the receptive field with uncertainty guidance for both quality and bitrate scalable compression. Lee *et al.* [30] propose to encode the latent representations into a compressed bitstream trip-plane to support fine-granular progressive compression. Jeon *et al.* [25] further improve this method with context-based trit-plane coding, increasing the R-D performance.

In contrast to these methods, in this work, we base our framework on VQGAN and combine it with the classical coding principle, to design a controllable generative compression framework that allows highly flexible and controllable bitrate adaption while generating plausible compressed images with solely one set of optimized weights.

3 Method

Our goal is to learn a unified generative compression model capable of compressing an image x for flexible and continuous bitrates while ensuring high perceptual fidelity. To this end, we propose Control-GIC, where the overview architecture is illustrated in Figure 3. Control-GIC contains three components: 1) granularity-informed encoder E to encode the image into variable-length codes; 2) statistical entropy coding module H for bitrate reduction; and 3) probabilistic conditional decoder D to reconstruct perceptually plausible results.

3.1 Correlation between Entropy and Information Density

Inspired by [11], we measure the information density of image regions based on a non-parametric spatial entropy algorithm. Unlike general feature-level entropy models [4, 5], our VQGAN-based model does not have the neural entropy model and is not optimized for entropy during training. We choose the non-parametric algorithm to reduce computational overhead while achieving good granularity selection performance. The mathematical representation process is as follows:

Assume $x \in \Omega$ is a pixel with a value p_x in $[-1,1]$, where Ω is a patch of the image. We define the pixel value bin $i = -1 + \frac{2k}{n-1}$, where $k = 0, 1, 2, \dots, n-1$, and the number of bins n is set to 32. We compute the Gaussian distance $f_{x,i}$ of x to each i , where σ is the standard deviation, see Eq. (1). Thus $f_{x,i}$ exhibits an unnormalized truncated discrete Gaussian distribution along i . It implies that we hypothesize a probability $f_{x,i}$, indicating the potential diffusion of p_x to i .

$$f_{x,i} = \exp\left(-\frac{(p_x - i)^2}{2\sigma^2}\right), \quad (1)$$

We average $f_{x,i}$ in the patch Ω to get the probability distribution $f_{\Omega,i}$ of this region, and normalize it to get $\overline{f_{\Omega,i}}$. We denote the average operation as “ $\text{mean}_{x \in \Omega}$ ”. The formulation is as follows:

$$\overline{f_{\Omega,i}} = \frac{f_{\Omega,i}}{\sum_j f_{\Omega,j}}, \quad \text{where } f_{\Omega,i} = \text{mean}_{x \in \Omega} f_{x,i}. \quad (2)$$

Finally, we use the following formulation to compute the spatial entropy $H(\Omega)$ of the patch Ω .

$$H(\Omega) = -\sum_i \overline{f_{\Omega,i}} \log \overline{f_{\Omega,i}}. \quad (3)$$

Control-GIC considers the entropy of local patches as the basis of the information density distribution of the image, and divides it into multiple non-overlapped patches sorted by their entropy value from low to high, which are then transformed into multi-grained features. The corresponding patch sizes required for entropy calculation are $\{4, 8, 16\}$, as detailed in Figure 2.

3.2 Granularity-Informed Encoder

The granularity-informed encoder E distills hierarchical features according to the determined entropy-based granularity assignments. These features are then integrated to form a multi-grained hybrid feature. Specifically, as visualized in Figure 3, given an input image $x \in \mathbb{R}^{H \times W \times 3}$, E distills x into features of three granularities: fine-grained $z_1 \in \mathbb{R}^{\frac{H}{4} \times \frac{W}{4} \times d}$, medium-grained $z_2 \in \mathbb{R}^{\frac{H}{8} \times \frac{W}{8} \times d}$,



Figure 2: Entropy values are visually represented in the middle column, with darker red pixels signifying higher entropy levels. We select regions of minimal entropy for coarse-grained representation, while areas with higher entropy, indicating greater information density, are allocated to finer-grained representations.

and coarse-grained $z_3 \in \mathbb{R}^{\frac{H}{16} \times \frac{W}{16} \times d}$. Based on the user-given ratios $(r_1, r_2, r_3) \in [0, 1]$ for three granularities, E extracts the elements with lowest r_i proportion of the entropy from z_i and generates binary masks $m_i \in \{0, 1\}$ at the same scale as z_i to indicate the position of extracted elements, where $i = 1, 2, 3$. This process is executed from coarse to fine, assigning the multi-grained representations progressively and finely. Subsequently, the continuous values in each z_i in $\{z_i\}_{i=1}^3$ are quantized against C to produce the quantized counterparts \hat{z}_i and a set of discrete indices Ind_i that represent the closest matches in C based on the Euclidean distance. This quantization step $\mathbf{q}(\cdot)$ is mathematically formalized as:

$$\begin{cases} \hat{z}_i = \mathbf{q}(z_i) = \arg \min_{c_k \in C} \|z_i - c_k\|, \\ Ind_i = k. \end{cases} \quad (4)$$

The hybrid multi-grained representation \hat{z} is constructed to match the spatial scale of the finest granularity, detailed in Eq. (5), where $(\cdot) \uparrow_4$ and $(\cdot) \uparrow_2$ signify upsampling operations that amplify the spatial dimensions by factors of 4 and 2, respectively. \odot is element-wise multiplication along the spatial dimension. The upsampling operation is the nearest neighbor interpolation that employs replicates values of feature points along both the width and height, ensuring that the original local structure integrity of each feature point is maintained.

$$\hat{z} = (\hat{z}_1 \odot m_1) + (\hat{z}_2 \odot m_2) \uparrow_2 + (\hat{z}_3 \odot m_3) \uparrow_4. \quad (5)$$

3.3 Probabilistic Conditional Decoder

In the context of the decoder within an autoencoder architecture, the latent representation y_i at layer i is reconstructed by integrating information from all preceding layers, starting from the initial input y_1 up to the output of the previous layer y_{i-1} . This reconstruction is formalized through the conditional probability, where y_i is distributed according to $p(y_i | y_{i-1}, \dots, y_2, y_1)$, capturing the likelihood of y_i given the history of latent representations. The more accurate the previous latent representations are, the more accurate y_i is, which further influence the overall quality of the image reconstruction.

According to Eq. (4), given the indices and corresponding masks indicating the codes of three granularities, we can losslessly reconstruct the multi-gained representation \hat{z} in the decoder end. While the upsampled components \hat{z}_2 and \hat{z}_3 maintain their local structure through direct value duplication as shown in Eq. (5), their global structure differs. Feeding \hat{z} directly into the decoder layers results in further loss of information.

Based on these considerations, we introduce a probabilistic conditional decoder specifically tailored for the initial layers of the decoder. This decoder employs $(\cdot) \downarrow_4$ and $(\cdot) \downarrow_2$ consisting of a $4 \times$ and a $2 \times$ average pooling layer to downscale \hat{z} back to the $\{\hat{z}_i \odot m_i\}_{i=1}^3$ losslessly. We provide $(\hat{z}) \downarrow_4$ as decoder input y_1 which contains the same $\hat{z}_3 \odot m_3$ as the encoder output to ensure the accuracy of the input. $\hat{z}_1 \odot m_1$ and $\hat{z}_2 \odot m_2$ are provided as conditions to y_2 and y_3 , respectively. These conditions serve as additional guidance for the reconstruction process which is formalized as:

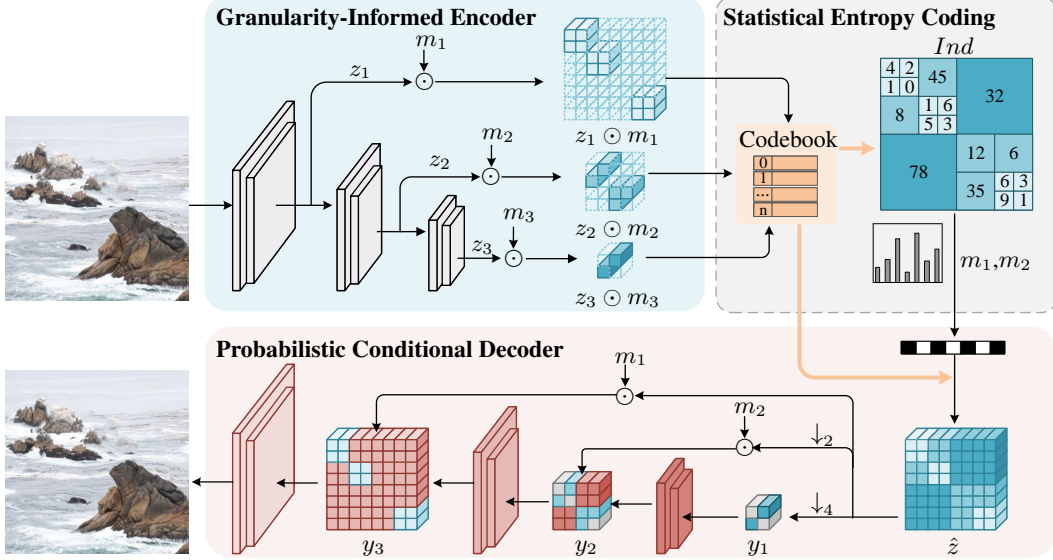


Figure 3: The overall framework of our Control-GIC. In the figure, all components cooperate for efficient compression with end-to-end training, and dashed lines represent the unparameterized entropy coding module. The symbols in the diagram are defined as: m : the binary mask; $(\cdot)_{\downarrow}$: average pooling operation; \odot : element-wise multiplication.

$$\begin{aligned} y_2 &\sim p(y_2 | y_1, (\hat{\mathbf{z}})_{\downarrow 2} \odot \mathbf{m}_2) \\ y_3 &\sim p(y_3 | y_2, y_1, \hat{\mathbf{z}} \odot \mathbf{m}_1) \end{aligned} \quad (6)$$

Specifically, the decoding process is detailed in Eq. (7), D begin with the $(\cdot)_{\downarrow 4}$ operation on $\hat{\mathbf{z}}$ to produce y_1 . The first decoder layer D_1 processes y_1 and generates y_2 in which $y_2 \odot m_2$ are deliberately replaced with the medium-grained representation $(\hat{\mathbf{z}})_{\downarrow 2} \odot m_2$ (equal to $\hat{\mathbf{z}} \odot m_2$). After that, D_3 condition with the $\hat{\mathbf{z}} \odot m_1$ and replace the unexact $y_3 \odot (1 - m_1)$, ensuring the precision of features in deep layers. This systematic replacement of representations at varying granularities with increasingly precise conditions progressively refines the latent space representation, helping D diminish information loss and substantially elevate the accuracy of the reconstructed images.

$$\begin{cases} y_1 &= (\hat{\mathbf{z}})_{\downarrow 4} \\ y_2 &= D_1(y_1) \odot (1 - m_2) + (\hat{\mathbf{z}})_{\downarrow 2} \odot \mathbf{m}_2 \\ y_3 &= D_2(y_2) \odot (1 - m_1) + \hat{\mathbf{z}} \odot \mathbf{m}_1 \\ \hat{\mathbf{x}} &= D_3(y_3) \end{cases} \quad (7)$$

3.4 Statistical Entropy Coding Strategy

The decoding process requires these pieces of bitstreams: the three granularity indices $\{Ind_i\}_{i=1}^3$, along with their corresponding masks $\{m_1, m_2\}$. These elements are encoded using lossless coding algorithms. The mask consisting of 0 and 1, is encoded directly into a binary stream. The indices, which point to codebook entries, exhibit an uneven frequency distribution, with a minority of codes being used for quantization [53]. To optimize indices' encoding, we introduce a statistical entropy coding strategy that captures the frequency distribution of indices usage across a natural dataset during training. Each index starts with a frequency count of 0, while the frequency is updated each time it is matched for vector quantization. To simulate the data distribution in the inference process, we utilize the last epoch's frequency statistics to construct a frequency table tailored for Huffman coding. We denote the bitrate after coding as $\mathcal{R}(\cdot)$, then the total bitrate of the entire image can be formulated as:

$$\mathcal{R} = \sum_{i=1}^3 \mathcal{R}(Ind_i) + \mathcal{R}(m_1) + \mathcal{R}(m_2), \quad (8)$$

Note that our model does not optimize network parameters specifically for bitrate. During inference, we control the bitrate using different multi-granularity allocation ratios. Specifically, we set a group of hyperparameters $\{r_1, r_2, r_3\}$ to represent the allocation ratios of the masks $\{m_1, m_2, m_3\}$ at various granularities. Since the bitrate is only related to the granular representations of local patches, we can flexibly determine the statistics of the granularities based on the entropy values to achieve dynamic adaption, achieving dynamic adaption in a target of the quality-bitrate adaptive manner in a unified model without any post-training. See Appendix A.3 for the bit-saving experiment of the statistical entropy coding.

3.5 Loss Function

The loss function \mathcal{L} for our approach contains the loss associated with the VQVAE architecture and GAN component. The optimization objective of $\mathcal{L}_{VQVAE}(E, G, C)$ is twofold: to minimize the distortion between the original inputs x and their reconstructions \hat{x} , and to reduce the divergence between the continuous representations $z = E(x)$ and their quantized versions \hat{z} , as shown in Eq. (9). The distortion of x is measured by MSE (d_M) and LPIPS (d_P). Due to the non-differentiable nature of quantization, the stop-gradient operation $sg[\cdot]$ is widely utilized in VQ-based models which enables the quantized representations \hat{z} to propagate gradients directly for optimizing the codebook C , and allows the continuous representations z to receive gradients for the refinement of the encoder E . We fine-tune the balance between these objectives using a hyperparameter β .

Our Control-GIC diverges from the conventional R-D optimization paradigm with no-parametric indices compression, enabling the model to adapt to different types of data and desired quality levels, rather than being constrained by a fixed R-D trade-off.

$$\begin{aligned} \mathcal{L}_{VQVAE}(E, G, C) &= \beta d(x, \hat{x}) + d(z, \hat{z}) \\ &= \beta(d_M + d_P)(x, \hat{x}) + \|sg[z] - \hat{z}\|_2^2 + \|sg[\hat{z}] - z\|_2^2 \end{aligned} \quad (9)$$

We use a hyperparameter β to control the trade-off between VQVAE and GAN. The GAN loss and the total loss \mathcal{L} is as follows:

$$\mathcal{L}_{GAN}(\{E, G, C\}, D) = \mathbb{E}_{x \sim p(x)} [\log D(x) + \log(1 - D(G(\hat{z})))] \quad (10)$$

$$\mathcal{L} = \mathcal{L}_{VQVAE} + \lambda \mathcal{L}_{GAN} \quad (11)$$

4 Experiment

4.1 Experimental Setup

Our method is based on MoVQ [55] which improves the VQGAN model by adding spatial variants into the decoder’s representation maps, avoiding the repeat artifact in neighboring patches. We leverage MoVQ’s pre-trained codebook and redesign the architecture to suit the compression objective.

Training & Inference Our training dataset consists of random 300k images from the OpenImages [29] dataset. We randomly crop images to a uniform 256×256 resolution. Within our model, we take three representation granularities: 4×4 , 8×8 , and 16×16 . The codebook $C \in \mathbb{R}^{k \times d}$ comprises $k = 16384$ code vectors, each with a dimension of $d = 4$. We train the model for 165k iterations with the learning rate of 5×10^{-5} on 4 NVIDIA RTX 3090 GPUs. Throughout the training, we maintain the ratio setting of (0.5, 0.4, 0.1) for the fine, medium, and coarse granularity, respectively. During inference, our controllable multi-granularity approach accepts any-resolution images and enables fine bitrate adjustment with a unified model.

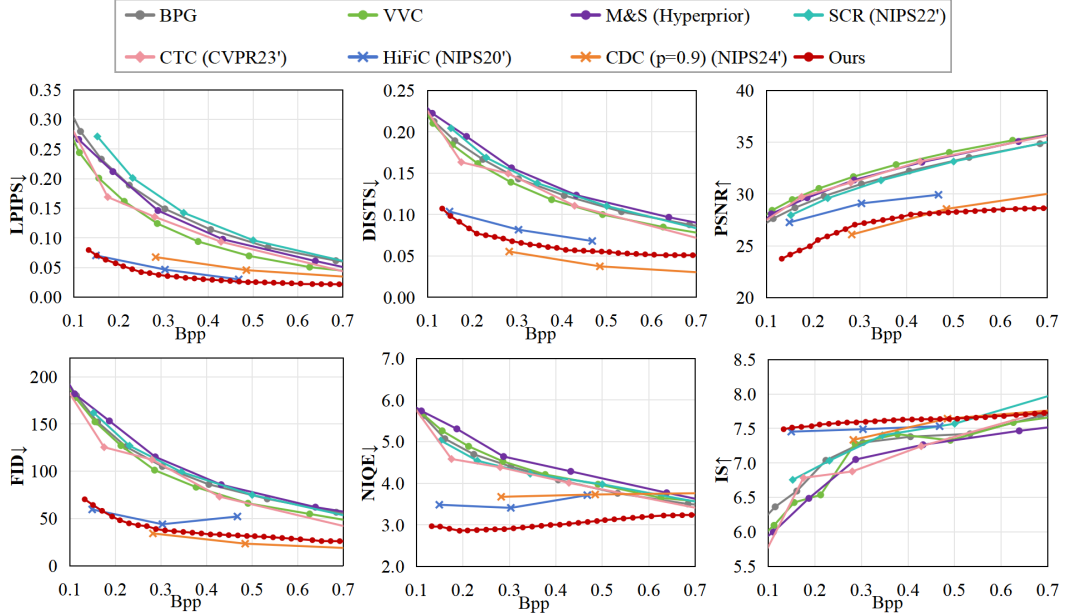


Figure 4: Compression performance with compared methods. In this figure, the lines with forks represent GIC methods, and the lines with rhombus represent progressive and variable-rate methods.

Evaluation We evaluate our method on Kodak [28] dataset, a standard in compression assessment, which contains 24 high-quality images at 768×512 resolution. We carry out multi-dimensional evaluation and utilize a comprehensive set of evaluation metrics including perceptual metrics: **LPIPS** [54], **DISTS** [16], distortion metric: **PSNR**, generative metrics: **FID** [21], **IS** [6], as well as the no-reference measurement: **NIQE** [39] to thoroughly assess the performance of our method. More details of metrics are in the Appendix A.2.

4.2 Performance Comparison

We evaluate our approach with recent state-of-the-art (SOTA) NIC methods. In terms of generative compression approaches, **1) HiFiC** [36] is an influential approach leveraging conditional GAN and taking rate-distortion-perception trade-off. **2) CDC** [51] is a representative diffusion-based lossy compression approach providing a compression performance that rivals GAN-based methods. Besides, we compare our Control-GIC with SOTA variable-rate and progressive neural compression methods in which images under various bitrates are generated by a unified network. **3) SCR** [32] proposes a 3D important map adjusted by quality level to decide the selected representation elements leading to variable-rate NIC. **4) CTC** [26] progressively decodes the bit stream which can be truncated at any point to finely regulate the bitrate. We utilize **BPG** (YUV444, x265 HEVC, 8-bit depth) [7] and **VVC** (VTM10.0) [9] as compared traditional codecs and **M&S (Hyperprior)** [37] as the classical NIC method for reference. For a fair comparison, we utilize a CDC version that the lpips weight $p = 0.9$ which is the endpoints close to the perception quality. We employ our unified model, getting the results of all bitrates with a single trained model, the ability to finely control the bit rate is reflected in the Appendix A.4.

Figure 4 demonstrates that our Control-GIC surpasses the majority of SOTA NIC methods and all traditional codecs across six distinct metrics. Our methodology exhibits a significant improvement in LPIPS, NIQE, and IS performance, approaching the SOTA performance of the CDC in terms of the FID with our unified model. Appendix A.1 presents more comparison results on high-resolution images.

While PSNR is pivotal for pixel-level evaluation, we find that our methods excel in generating realistic images. This performance is notable even when compared to methods that are specifically optimized for pixel-level accuracy. Thus, we explore the quantitative comparison between our Control-GIC and the compared methods. As depicted in Figure 5, VVC, M&S (Hyperprior) as well

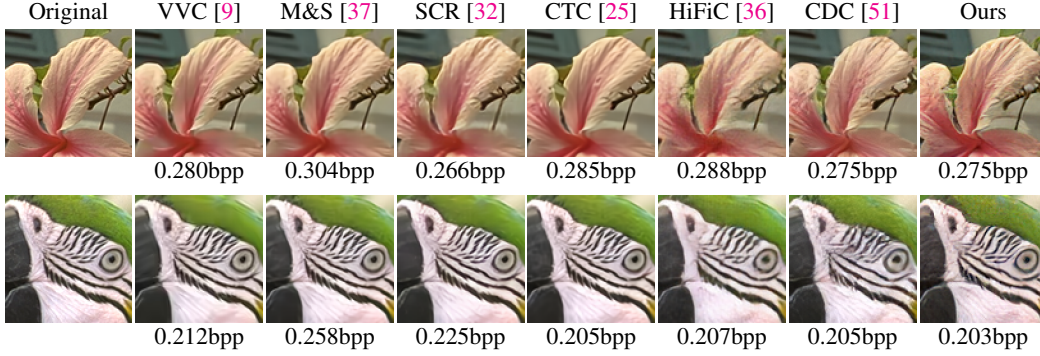


Figure 5: The quantitative comparison with the traditional VVC, classical learned M&S (Hyperprior), variable-rate method SCR, progressive method CTC, as well as the GIC methods HiFiC and CDC.

as variable-rate SCR and progressive CTC exhibit noticeable issues with blurred artifacts and detail loss, and generative HiFiC and CDC generate artifacts that were not originally present in the images. Compared to them, our method demonstrates superior performance in preserving texture integrity and image sharpness for a great visual experience.

4.3 Efficiency of Probabilistic Conditional Decoder

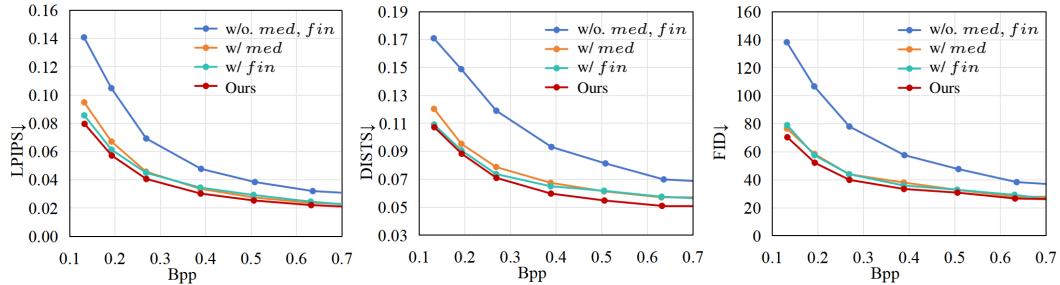


Figure 6: The ablation experiments on multi-grained conditions for the probabilistic conditional decoder.

Based on the theoretical analysis of the probabilistic conditional decoder, we explore the contribution of the conditions: the medium-grained $(\hat{z})_{\downarrow 2} \odot m_2$ (denoted as *med*) and fine-grained $\hat{z} \odot m_1$ (denoted as *fin*) to the decoder in Eq. (7). We train all the models for the same iterations and evaluate the performance on both perceptual and generative quality measurements. Figure 6 demonstrates that the model without the *med* and *fin* exhibits the worst results in three metrics. Both *med* and *fin* have a significant improvement in model performance, and conditioning on both of them presents the best results, especially on DISTSI. It can be observed that adding the fine-grained *fin* to the model brings more benefits than adding *med*, which is because the fine-grained *fin* corrects the features in deeper decoder layers, ensuring the accuracy of features after multiple nonlinear transformations of the decoder.

5 Conclusion

Our proposed Control-GIC framework addresses the critical challenge of flexible rate adaption in generative image compression. By leveraging a VQGAN foundation and correlating local image information density with granular representations, Control-GIC achieves fine-grained bitrate control across a wide range while maintaining high-fidelity compression performance. The innovative probabilistic conditional decoder enhances reconstruction realism by aggregating hierarchical features informed by conditional probability. Our experiments validate the superior adaptability and performance of Control-GIC, showcasing its capability for efficient compression and bit control, outperforming recent state-of-the-art methods.

6 Limitations

Our Control-GIC unleashes the capabilities of the VQGAN model, delivering high-quality reconstruction across a broad range of bitrates, and outperforming traditional MSE-optimized methods in visual performance. However, it is important to recognize that at higher bitrates, specifically above 1.0 bpp, our method encounters limitations. MSE-optimized algorithms excel in preserving fine details and textures at these bitrates due to their focus more on subtle distortions. Thus GIC methods, including ours, may not match the detail precision achievable by MSE-optimized techniques.

References

- [1] Eirikur Agustsson and Radu Timofte. Ntire 2017 challenge on single image super-resolution: Dataset and study. In *2017 IEEE Conference on Computer Vision and Pattern Recognition Workshops (CVPRW)*, pages 1122–1131, 2017.
- [2] Eirikur Agustsson, Michael Tschannen, Fabian Mentzer, Radu Timofte, and Luc Van Gool. Generative adversarial networks for extreme learned image compression. In *Proceedings of the IEEE/CVF International Conference on Computer Vision*, pages 221–231, 2019.
- [3] Yuanchao Bai, Xianming Liu, Wangmeng Zuo, Yaowei Wang, and Xiangyang Ji. Learning scalable ly=-constrained near-lossless image compression via joint lossy image and residual compression. In *Proceedings of the IEEE Conference on Computer Vision and Pattern Recognition*, pages 11946–11955, 2021.
- [4] Johannes Ballé, Valero Laparra, and Eero P. Simoncelli. End-to-end optimized image compression. In *International Conference on Learning Representations*, 2017.
- [5] Johannes Ballé, David Minnen, Saurabh Singh, Sung Jin Hwang, and Nick Johnston. Variational image compression with a scale hyperprior. *arXiv preprint arXiv:1802.01436*, 2018.
- [6] Shane Barratt and Rishi Sharma. A note on the inception score. *arXiv preprint arXiv:1801.01973*, 2018.
- [7] Fabrice Bellard. BPG Image format. <https://bellard.org/bpg/>.
- [8] Yochai Blau and Tomer Michaeli. Rethinking lossy compression: The rate-distortion-perception tradeoff. In *International Conference on Machine Learning*, pages 675–685. PMLR, 2019.
- [9] Benjamin Bross, Jianle Chen, Jens-Rainer Ohm, Gary J Sullivan, and Ye-Kui Wang. Developments in international video coding standardization after avc, with an overview of versatile video coding (vvc). *Proceedings of the IEEE*, 109(9):1463–1493, 2021.
- [10] Chunlei Cai, Li Chen, Xiaoyun Zhang, and Zhiyong Gao. Efficient variable rate image compression with multi-scale decomposition network. *IEEE Transactions on Circuits and Systems for Video Technology*, 29(12):3687–3700, 2019.
- [11] Turgay Celik. Spatial entropy-based global and local image contrast enhancement. *IEEE Transactions on Image Processing*, 23(12):5298–5308, 2014.
- [12] Tong Chen and Zhan Ma. Variable bitrate image compression with quality scaling factors. In *ICASSP 2020-2020 IEEE International Conference on Acoustics, Speech and Signal Processing (ICASSP)*, pages 2163–2167. IEEE, 2020.
- [13] Zhengxue Cheng, Heming Sun, Masaru Takeuchi, and Jiro Katto. Learned image compression with discretized gaussian mixture likelihoods and attention modules. In *Proceedings of the IEEE/CVF conference on computer vision and pattern recognition*, pages 7939–7948, 2020.
- [14] Yoojin Choi, Mostafa El-Khamy, and Jungwon Lee. Variable rate deep image compression with a conditional autoencoder. In *Proceedings of the IEEE International Conference on Computer Vision*, pages 3146–3154, 2019.
- [15] Ze Cui, Jing Wang, Shangyin Gao, Tiansheng Guo, Yihui Feng, and Bo Bai. Asymmetric gained deep image compression with continuous rate adaptation. In *Proceedings of the IEEE/CVF Conference on Computer Vision and Pattern Recognition*, pages 10532–10541, 2021.
- [16] Keyan Ding, Kede Ma, Shiqi Wang, and Eero P Simoncelli. Image quality assessment: Unifying structure and texture similarity. *IEEE transactions on pattern analysis and machine intelligence*, 44(5):2567–2581, 2020.
- [17] Patrick Esser, Robin Rombach, and Bjorn Ommer. Taming transformers for high-resolution image synthesis. In *Proceedings of the IEEE/CVF conference on computer vision and pattern recognition*, pages 12873–12883, 2021.
- [18] Ian Goodfellow, Jean Pouget-Abadie, Mehdi Mirza, Bing Xu, David Warde-Farley, Sherjil Ozair, Aaron Courville, and Yoshua Bengio. Generative adversarial nets. *Advances in neural information processing systems*, 27, 2014.

- [19] Sha Guo, Zhuo Chen, Yang Zhao, Ning Zhang, Xiaotong Li, and Lingyu Duan. Toward scalable image feature compression: A content-adaptive and diffusion-based approach. In *Proceedings of the 31st ACM International Conference on Multimedia*, pages 1431–1442, 2023.
- [20] Wang Guo-Hua, Jiahao Li, Bin Li, and Yan Lu. EVC: Towards real-time neural image compression with mask decay. In *The Eleventh International Conference on Learning Representations*, 2023.
- [21] Martin Heusel, Hubert Ramsauer, Thomas Unterthiner, Bernhard Nessler, and Sepp Hochreiter. Gans trained by a two time-scale update rule converge to a local nash equilibrium. *Advances in neural information processing systems*, 30, 2017.
- [22] Jonathan Ho, Ajay Jain, and Pieter Abbeel. Denoising diffusion probabilistic models. *Advances in neural information processing systems*, 33:6840–6851, 2020.
- [23] Emiel Hoogeboom, Alexey A Gritsenko, Jasmijn Bastings, Ben Poole, Rianne van den Berg, and Tim Salimans. Autoregressive diffusion models. In *International Conference on Learning Representations*, 2021.
- [24] Shoma Iwai, Tomo Miyazaki, and Shinichiro Omachi. Controlling rate, distortion, and realism: Towards a single comprehensive neural image compression model. In *Proceedings of the IEEE/CVF Winter Conference on Applications of Computer Vision*, pages 2900–2909, 2024.
- [25] Seungmin Jeon, Kwang Pyo Choi, Youngo Park, and Chang-Su Kim. Context-based trit-plane coding for progressive image compression. In *Proceedings of the IEEE Conference on Computer Vision and Pattern Recognition*, pages 14348–14357, 2023.
- [26] Seungmin Jeon, Kwang Pyo Choi, Youngo Park, and Chang-Su Kim. Context-based trit-plane coding for progressive image compression. In *Proceedings of the IEEE Conference on Computer Vision and Pattern Recognition*, 2023.
- [27] Nick Johnston, Damien Vincent, David Minnen, Michele Covell, Saurabh Singh, Troy Chinen, Sung Jin Hwang, Joel Shor, and George Toderici. Improved lossy image compression with priming and spatially adaptive bit rates for recurrent networks. In *Proceedings of the IEEE conference on computer vision and pattern recognition*, pages 4385–4393, 2018.
- [28] Eastman Kodak. Kodak lossless true color image suite (photocd pcd0992), 1993. <http://r0k.us/graphics/kodak/>.
- [29] Ivan Krasin, Tom Duerig, Neil Alldrin, Vittorio Ferrari, Sami Abu-El-Haija, Alina Kuznetsova, Hassan Rom, Jasper Uijlings, Stefan Popov, Andreas Veit, et al. Openimages: A public dataset for large-scale multi-label and multi-class image classification. *Dataset available from <https://github.com/openimages>*, 2(3):18, 2017.
- [30] Jae-Han Lee, Seungmin Jeon, Kwang Pyo Choi, Youngo Park, and Chang-Su Kim. Dpict: Deep progressive image compression using trit-planes. In *Proceedings of the IEEE Conference on Computer Vision and Pattern Recognition*, pages 16113–16122, 2022.
- [31] Jooyoung Lee, Seunghyun Cho, and Seung-Kwon Beack. Context-adaptive entropy model for end-to-end optimized image compression. *arXiv preprint arXiv:1809.10452*, 2018.
- [32] Jooyoung Lee, Seyoon Jeong, and Munchurl Kim. Selective compression learning of latent representations for variable-rate image compression. *Advances in Neural Information Processing Systems*, 35:13146–13157, 2022.
- [33] Yadong Lu, Yin hao Zhu, Yang Yang, Amir Said, and Taco S Cohen. Progressive neural image compression with nested quantization and latent ordering. In *2021 IEEE International Conference on Image Processing (ICIP)*, pages 539–543. IEEE, 2021.
- [34] Qi Mao, Tinghan Yang, Yinuo Zhang, Shuyin Pan, Meng Wang, Shiqi Wang, and Siwei Ma. Extreme image compression using fine-tuned vqgan models. *arXiv preprint arXiv:2307.08265*, 2023.
- [35] Yixin Mei, Li Li, Zhu Li, and Fan Li. Learning-based scalable image compression with latent-feature reuse and prediction. *IEEE Transactions on Multimedia*, 24:4143–4157, 2022.
- [36] Fabian Mentzer, George D Toderici, Michael Tschannen, and Eirikur Agustsson. High-fidelity generative image compression. *Advances in Neural Information Processing Systems*, 33:11913–11924, 2020.
- [37] David Minnen, Johannes Ballé, and George D Toderici. Joint autoregressive and hierarchical priors for learned image compression. *Advances in neural information processing systems*, 31, 2018.
- [38] David Minnen and Saurabh Singh. Channelwise autoregressive entropy models for learned image compression. In *2020 IEEE International Conference on Image Processing*, pages 3339–3343. IEEE, 2020.
- [39] Anish Mittal, Rajiv Soundararajan, and Alan C Bovik. Making a “completely blind” image quality analyzer. *IEEE Signal processing letters*, 20(3):209–212, 2012.
- [40] Yichen Qian, Ming Lin, Xiuyu Sun, Zhiyu Tan, and Rong Jin. Entroformer: A transformer-based entropy model for learned image compression. In *International Conference on Learning Representations*, 2022.

- [41] Oren Rippel and Lubomir Bourdev. Real-time adaptive image compression. In *International Conference on Machine Learning*, pages 2922–2930. PMLR, 2017.
- [42] Shibani Santurkar, David Budden, and Nir Shavit. Generative compression. In *2018 Picture Coding Symposium (PCS)*, pages 258–262. IEEE, 2018.
- [43] Claude E Shannon et al. Coding theorems for a discrete source with a fidelity criterion. *IRE Nat. Conv. Rec.*, 4(142-163):1, 1959.
- [44] David S. Taubman and Michael W. Marcellin. *JPEG 2000: Image Compression Fundamentals, Standards and Practice*. Kluwer Academic Publishers, Norwell, MA, USA, 2001.
- [45] George Toderici, Sean M. O’Malley, Sung Jin Hwang, Damien Vincent, David Minnen, Shumeet Baluja, Michele Covell, and Rahul Sukthanka. Variable rate image compression with recurrent neural networks. In *Proceedings of the International Conference on Learning Representations*, pages 1–12, 2016.
- [46] George Toderici, Damien Vincent, Nick Johnston, Sung Jin Hwang, David Minnen, Joel Shor, and Michele Covell. Full resolution image compression with recurrent neural networks. In *Proceedings of the IEEE conference on Computer Vision and Pattern Recognition*, pages 5306–5314, 2017.
- [47] Michael Tschannen, Eirikur Agustsson, and Mario Lucic. Deep generative models for distribution-preserving lossy compression. *Advances in neural information processing systems*, 31, 2018.
- [48] Gregory K Wallace. Overview of the jpeg (isoccitt) still image compression standard. In *Image Processing Algorithms and Techniques*, volume 1244, pages 220–233. SPIE, 1990.
- [49] Yueqi Xie, Ka Leong Cheng, and Qifeng Chen. Enhanced invertible encoding for learned image compression. In *Proceedings of the ACM International Conference on Multimedia*, pages 162–170, 2021.
- [50] Fei Yang, Luis Herranz, Yongmei Cheng, and Mikhail G. Mozerov. Slimmable compressive autoencoders for practical neural image compression. In *Proceedings of the IEEE Conference on Computer Vision and Pattern Recognition*, pages 4998–5007, 2021.
- [51] Ruihan Yang and Stephan Mandt. Lossy image compression with conditional diffusion models. *Advances in Neural Information Processing Systems*, 36, 2024.
- [52] Dongyi Zhang, Feng Li, Man Liu, Runmin Cong, Huihui Bai, Meng Wang, and Yao Zhao. Exploring resolution fields for scalable image compression with uncertainty guidance. *IEEE Transactions on Circuits and Systems for Video Technology*, 34(4):2934–2948, 2024.
- [53] Jiahui Zhang, Fangneng Zhan, Christian Theobalt, and Shijian Lu. Regularized vector quantization for tokenized image synthesis. In *Proceedings of the IEEE/CVF Conference on Computer Vision and Pattern Recognition*, pages 18467–18476, 2023.
- [54] Richard Zhang, Phillip Isola, Alexei A Efros, Eli Shechtman, and Oliver Wang. The unreasonable effectiveness of deep features as a perceptual metric. In *Proceedings of the IEEE/CVF Conference on Computer Vision and Pattern Recognition*, pages 586–595, 2018.
- [55] Chuanxia Zheng, Tung-Long Vuong, Jianfei Cai, and Dinh Phung. Movq: Modulating quantized vectors for high-fidelity image generation. *Advances in Neural Information Processing Systems*, 35:23412–23425, 2022.
- [56] Renjie Zou, Chunfeng Song, and Zhaoxiang Zhang. The devil is in the details: Window-based attention for image compression. In *Proceedings of the IEEE/CVF Conference on Computer Vision and Pattern Recognition*, pages 17492–17501, 2022.

A Supplemental Material - Once-for-All: Controllable Generative Image Compression with Dynamic Granularity Adaption

A.1 Performance Comparison on High-Resolution Images

In this section, we present a performance comparison on the DIV2K [1] validation dataset containing 100 high-resolution images. As depicted in Figure 7, we compare with traditional codecs, variable-rate NIC method as well as generative method (Note that the high-resolution image compression is not supported in CDC [51]), and employ six key metrics to assess the performance of the compression algorithms, including the perceptual metrics (LPIPS, DISTS), distortion metric (PSNR), generative metrics (FID, IS), and no-reference NIQE. These metrics collectively provide a comprehensive evaluation of the image compression quality and our Control-GIC achieves the best performance in a wide spectrum of bitrates.

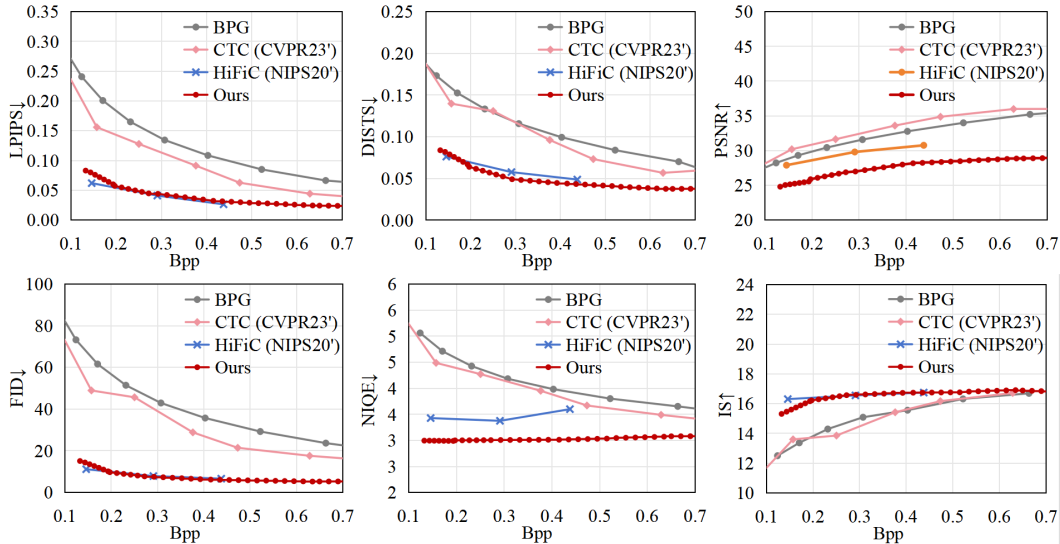


Figure 7: Compression performance in high-resolution images with compared methods. In this figure, the lines with forks represent GIC methods, and the lines with rhombus represent variable-rate methods.

A.2 Evaluation Metrics

we adopt a comprehensive set of evaluation metrics to thoroughly assess the performance of our image compression and reconstruction techniques. Our selection encompasses perceptual metrics, distortion metrics, generative metrics, and a no-reference metric, ensuring a multifaceted evaluation. The perceptual metrics include LPIPS [54], which measures the perceptual difference between images, and DISTS [16], which evaluates the structural dissimilarity. These metrics are crucial for understanding how closely compressed and reconstructed images resemble their original counterparts in terms of human visual perception. We also include the widely recognized distortion metric PSNR, which quantifies the pixel-level differences between the original and reconstructed images. PSNR is a standard in the field, providing a straightforward measure of image fidelity. For generative metrics, we employ FID (Fréchet Inception Distance) [21] to offer statistical assessments of the similarity between the distributions of original images and those of reconstructed images, which is particularly valuable in the context of generative models. Additionally, we incorporate IS (Inception Score) [6], which is another way to gauge the quality and diversity of generated images. NIQE (Natural Image Quality Evaluator) [39] stands out as a no-reference metric, capable of evaluating image quality without requiring an original reference image. This feature renders NIQE exceptionally beneficial in applications such as super-resolution where an original high-resolution image may not be available. For comparing with other methods on FID and IS, we split images on Kodak into 192 patches and DIV2K into 6 573 patches with a patch size of 256.

A.3 Bit Saving of Statistical Entropy Coding Strategy

In the Control-GIC method, the accurate reconstruction of images from compressed data is highly dependent on the lossless compression of indices, which determine the codes for decoding. To achieve this, we employ Huffman coding, an algorithm that efficiently compresses data by assigning shorter binary codes to elements that occur more frequently. However, using frequency statistics tailored to each individual image would require transmitting both the encoded bitstream and the mapping of elements to binary codes, incurring significant bit costs.

As described in Table 1, we compare our statistical entropy coding strategy with the classical ZIP compression algorithm and Huffman coding with uniform frequencies for each index. Our statistical entropy coding strategy brings 68.4%, 65.7%, and 59.0% bit savings compared to ZIP in the three granularity ratios, as well as 6.4%, 6.6%, and 8.2% bit savings compared to Huffman coding with uniform frequency for each code.

Table 1: Bit cost comparison of ZIP, Huffman coding with uniform frequency for each index, and our entropy coding strategy on the Kodak dataset. Our strategy counts the frequency of all indexes being used in the training process as a generalized and shared probability in the encoding and decoding process.

Granularity Ratio	ZIP	Huffman	Huffman (Ours)
		<i>w.</i> uniform frequency	<i>w.</i> statistical frequency
(0, 0.5, 0.5)	0.304	0.141	0.132
(0.1, 0.8, 0.1)	0.784	0.288	0.269
(0.5, 0.4, 0.1)	1.232	0.550	0.505

A.4 Fine Control of Bitrate

Our experiment with variable-rate control demonstrates the adaptive bitrate adjustment capabilities of our method as well as the corresponding quality changes across the bitrates, as measured by four different metrics, as detailed in Table 2. By fine-tuning the granularity ratio, we are able to make incremental adjustments to the bitrate. This results in a continuous range of bitrates that offer higher efficiency and flexibility with minimal impact on computational resources and processing time than single-rate models.

Table 2: The elastic and fine bitrate control presentation over the Kodak dataset at bitrates ranging from 0.389 to 0.391. All results are shown in five valid digits to represent differences more clearly. The Granularity Ratio refers to the proportion of fine granularity, medium granularity, and coarse granularity from left to right.

Granularity Ratio	Bpp↓	LPIPS↓	DISTS↓	FID↓	NIQE↓
(0.301, 0.599, 0.1)	0.38925	0.03027	0.05984	33.327	2.9975
(0.302, 0.598, 0.1)	0.38983	0.03025	0.05961	33.338	2.9971
(0.303, 0.597, 0.1)	0.39050	0.03020	0.05973	33.233	2.9967
(0.304, 0.596, 0.1)	0.39108	0.03014	0.05968	33.215	2.9942